HHS Public Access

Author manuscript

Acad Radiol. Author manuscript; available in PMC 2018 November 01.

Published in final edited form as:

Acad Radiol. 2018 November ; 25(11): 1388–1397. doi:10.1016/j.acra.2018.02.025.

Differentiation of Benign and Malignant Thyroid Nodules by Using Comb-push Ultrasound Shear Elastography: A Preliminary Two-plane View Study

Adriana Gregory[a], **Mahdi Bayat**[b], **Viksit Kumar**[b], **Max Denis**[a], **Bae Hyung Kim**[b], **Jeremy Webb**[a], **Duane D Meixner**[a], **Mabel Ryder**[c], **John M Knudsen**[a], **Shigao Chen**[a], **Mostafa Fatemi**[b], and **Azra Alizad**[a]

[a]Department of Radiology, Mayo Clinic College of Medicine, Rochester, Minnesota 55905, USA

[b]Department of Physiology and Biomedical Engineering, Mayo Clinic College of Medicine, Rochester, Minnesota 55905, USA

[c]Endocrinology, Department of Internal Medicine, Mayo Clinic College of Medicine, Rochester, Minnesota 55905, USA

Abstract

Rationale and Objectives—Low specificity of traditional ultrasound in differentiating benign from malignant thyroid nodules leads to a great number of unnecessary (i.e. benign) fine needle aspiration biopsies that causes a significant financial and physical burden to the patients. Ultrasound shear wave elastography is a technology capable of providing additional information related to the stiffness of tissues. In this study, quantitative stiffness values acquired by ultrasound shear wave elastography in two different imaging planes were evaluated for the prediction of malignancy in thyroid nodules. In addition, the association of elasticity measurements with sonographic characteristics of thyroid gland and nodules is presented.

Materials and Methods—A total number of 155 patients (106 female and 49 male) (average age 57.48±14.44 years) with 173 thyroid nodules (average size 24.89±15.41mm, range 5–68mm) scheduled for fine needle aspiration biopsy were recruited from March 2015 to May 2017. Comb-push shear elastography imaging was performed at longitudinal and transverse anatomical planes. Mean (E_{mean}) and maximum (E_{max}) elasticity values were obtained.

Results—Measurements at longitudinal view were statistically significantly higher than measurements at transverse view. Nodules with calcifications were associated with increased elasticity and nodules with a vascular component or within an enlarged thyroid gland (goiter) were associated with a lower elasticity value. Receiver operating characteristic curve analysis was performed for E_{mean} and E_{max} at each imaging plane and for the average of both planes. 95.45% sensitivity, 86.61% specificity, 0.58 PPV, and 0.99 NPV were achieved by the average of the two

Corresponding author: Azra Alizad, 200 First Street SW, Rochester, MN 55905, Phone: (507)538-1727, Alizad.Azra@mayo.edu.

Disclosure Statement

Mayo Clinic and SC have financial interest related to a device or technology referenced in this paper. AG, MB, VK, BHK, JW, DDM, MR, JMK, MF, and AA have no competing financial interests in the technology described in this study. The content is solely the responsibility of the authors and does not necessarily represent the official views of the National Institutes of Health.

planes for each E_{mean} and E_{max} parameters, with area under the curve of 92% and 93%, and a cutoff value of 49.09 kPa and 105.61 kPa, respectively.

Conclusions—The elastic properties of thyroid nodules showed promise to be a good discriminator between malignant and benign nodules ($p<0.0001$). However, probe orientation and internal features such as calcifications, vascular component and goiter may influence the final elastography measurements. A larger number of malignant nodules need to be studied to further validate our results.

Keywords

Shear Wave; Elastography; Thyroid nodules; Ultrasound; Cancer

Introduction

Thyroid nodules commonly grow inside the thyroid gland and are mostly benign. Only 4 to 6.5 percent of all thyroid nodules are cancerous (1). The majority of individuals with thyroid nodules have no symptoms. The nodules are usually found during routine physical examination with some incidental findings seen on diagnostic imaging (e.g., US, CT, MRI, or PET) performed for other indications (2). The current first line of evaluation of thyroid nodules encompasses thyroid hormone and thyroid-stimulating hormone laboratory tests, and ultrasonography of the thyroid gland. Ultrasonography is non-invasive and reveals many features relevant to the pathology of nodules. For example, an increased risk of malignancy has been associated with the presence of microcalcifications, irregular or spiculated margins with no halo, marked hypoechogenicity, mostly solid composition, and taller than wider shape. Although increased intranodular vascularity itself is not useful for differentiation of malignant from benign nodules (3–5), however, disordered central hypervascularity is more specific to US features of malignancy (6–8). On the other hand, presence of peripheral vascularity, round shape, isoechogenicity, spongiform appearance, smooth margins, and cystic composition are associated with benignancy (9–11).

Many studies have concluded that ultrasound features alone suffer from low accuracy. As such, fine needle aspiration (FNA) biopsy is often used to rule out cancer in thyroid nodules (5, 12). Although FNA is a safe and widely used procedure, complications such as discomfort and/or local pain and self-limited small hematomas may occur (13). Approximately 60% to 80% of FNAs result in benign findings (14–16).

Ultrasound shear wave elastography (SWE) is a commercially available technology that offers a new quantitative feature known as elasticity (17). Elasticity can be used for the discrimination of different types of tissues. This parameter is related to the stiffness of tissues, where high and low elasticity values denote hard and soft, respectively. Shear wave elastography has been broadly studied for the differentiation of benign and malignant breast masses (18, 19) and for staging of liver fibrosis (20, 21) with promising results. However, fewer studies have investigated the accuracy of SWE in the differentiation of benign and malignant thyroid nodules (22–27).

In this study, the elastography technique was comb-push ultrasound shear elastography (CUSE) (27–29), which uses multiple laterally distributed focused ultrasound beams simultaneously to induce shear waves in tissues and produce 2D elasticity maps. CUSE was performed and evaluated on 116 patients with 134 thyroid nodules at different probe orientations and considering the external and internal features of thyroid nodules. SWE results were compared to FNA biopsy outcomes.

Methods and Materials

Study population

This prospective study was approved by our Institutional Review Board and was HIPPA compliant. Patients scheduled for fine needle aspiration (FNA) biopsy of one or multiple thyroid nodules with a minimum age of 17 were recruited from March 2015 to May 2017. Thyroid nodules were selected for FNA biopsy based on the following ultrasound features: echogenicity (iso/hyperechoic, hypoechoic, and very hypoechoic), taller-than-wide, irregular-margins and presence of calcifications. In addition, nodule size and/or clinical context were evaluated. Low suspicion nodules measuring 1.5 cm or larger and intermediate or high suspicion nodules measuring 1.0 cm or larger were considered for FNA. Written informed consent was obtained from each participant prior to the study. A total of 176 patients were enrolled, 21 (11.9%) of which were excluded due to postponement of FNA biopsy (57.1%), lymph nodes (38.1%) and parathyroid (4.8%). 155 patients (106 female and 49 male; mean age, 56.19±13.88 years and 60.42±15.11 years, respectively) with 173 thyroid nodules constituted the study population.

US Shear Wave Elastography

For all patients, CUSE was performed before FNA biopsy. The study was conducted with the ultrasound scanner GE LOGIQ E9 with CUSE capability using a linear array transducer L-9 (GE Healthcare, Wauwatosa, WI). The imaging protocol consisted of few B-mode images followed by multiple SWE images, for both longitudinal and transverse cross-sections. The images were acquired by an expert sonographer with more than 30 years of clinical experience. A minimum of three SWE images was acquired per plane. SWE acquisitions that showed inconsistencies (i.e. due to patient or probe motion and pre-compression) were excluded prior to any analysis. Subsequently, elasticity measurements were performed on the three images for statistical analysis. A 3mm (in diameter) region of interest (ROI) was used to estimate the shear wave speed values. Multiple ROIs (up to three) were placed inside the nodule area seen on the B-mode image. The number of ROIs was determined by the size of the nodule: nodules between 5mm and 9mm had two ROIs, and nodules larger than 9mm had three ROIs. Thus, measurements from up to nine ROIs were calculated per cross-section for each nodule. Mean (E_{mean}) and maximum (E_{max}) elasticity values were captured for statistical analysis. All measurements were performed by one observer before FNA results were available for comparison.

During the study, minimum compression was applied with the ultrasound probe on the patient to prevent compression effects. For each acquisition, the patient was asked to hold his/her breath for about 3 seconds during which SWE images were acquired. In cases where

nodules presented a solid component (i.e. calcifications) or a fluid component (i.e. cystic region), SWE was performed (if available) solely on the soft tissue component of the nodule, this approach was compliant with the WFUMB guidelines (30). For the first 9 patients (9 nodules) enrolled in the study, SWE was acquired only at one probe orientation (5 at longitudinal and 4 at transverse).

Statistical Analysis

The statistical analysis was performed using the software JMP (SAS Institute Ver. 10.0.0) and MedCalc (MedCalc Software bvba Ver. 15.8, Belgium). Average of E_{mean} and average of E_{max} values from the ROIs were calculated per image. Then, the median of the averaged E_{mean} and median of averaged E_{max} values across the three images were estimated per plane; these parameters are represented as E_{mean}-L, E_{mean}-T, E_{max}-L, and E_{max}-T (L: longitudinal, T: transverse). In addition, the average of the medians of both planes was calculated as E_{mean}-L∩T and E_{max}-L∩T, and all measurements were included as E_{mean}-L∪T, and E_{max}-L∪T (i.e., adding nodules with measurements at only one plane). Receiver operating characteristic curve analysis was performed for all the above mentioned parameters. The cutoff value was selected at the maximum sensitivity, specificity, and area under the curve (AUC). A two tailed Student's t-test or Mann-Whitney test was used to compare the mean and maximum elasticity of thyroid nodules based on pathological results, features of the thyroid gland, nodule composition, and nodule size. Statistical significance was considered at $p<0.05$. The intraclass correlation coefficient was calculated for mean and maximum elasticity values to assess resemblance between the three SWE images at longitudinal and transverse cross-sections.

Results

Pathology

After FNA biopsy, 112 (83.58%) nodules were diagnosed as benign (Bethesda II) and 22 (16.42%) as malignant (Bethesda VI). The remaining thyroid nodules resulted in 15 nodules Bethesda I, 1 nodule Bethesda III, 20 nodules Bethesda IV, and 3 nodules Bethesda V. From the malignant group, 19 (86.36%) nodules were papillary thyroid carcinoma, 2 (9.09%) nodules were metastatic papillary carcinoma, and 1 (4.55%) nodule was Hurthle cell carcinoma. From the entire cohort, 37 (23.87%) patients had goiter (30 nodules were benign, 2 nodules were Bethesda I, 6 nodules were Bethesda IV, and 1 nodule was malignant). 2 (1.29%) patients had Graves' disease (the 3 studied nodules were benign). 3 (1.94%) patients who previously underwent complete thyroidectomy presented with new nodules on the thyroid bed (2 nodules were recurrent thyroid carcinoma and 1 nodule was Bethesda I). Figure 1 shows the shear wave speed map of a recurrent Hurthle cell carcinoma.

Repeatability Analysis

Intraclass correlation coefficients of the mean and maximum elasticity measurements at longitudinal orientation were 0.95 (CI: 0.94–0.96) and 0.88 (CI: 0.85–0.91), respectively; and at transverse orientation were 0.91 (CI: 0.89–0.93) and 0.85 (CI: 0.81–0.89), respectively. These results show low variability between the three elasticity maps of thyroid nodules at each imaging plane.

SWE Results compared to Sonographic Pattern and FNA Cytology

All nodules were categorized based on their sonographic pattern and the Bethesda system for thyroid cytopathology following the American Thyroid Association guidelines for management of thyroid nodules (5). Table 1 shows the results obtained from CUSE for mean and maximum elasticity values compared to the sonographic pattern and FNA cytology findings.

Bethesda category VI with low, intermediate and high sonographic suspicion and Bethesda category V with intermediate sonographic suspicion showed higher E_{mean} and E_{max} values in comparison to lower Bethesda categories. Similarly, very low suspicion sonographic pattern showed lower E_{mean} and E_{max} values. Nevertheless, high, intermediate and low suspicion sonographic pattern presented a wide range of E_{mean} and E_{max} results for each classification.

SWE and Probe Orientation

From 173 nodules, the first 14 nodules (from 13 patients) were evaluated with SWE only in one imaging plane (8 nodules were evaluated in longitudinal plane and 6 nodules in transverse plane). The subsequent 159 nodules were imaged in both anatomic planes, from which 3 nodules showed a blank SWE map at transverse plane. The blank map was attributed to the low penetration of shear waves due to the deep location of the nodules (nodule depth>3.5cm); therefore, no measurements could be obtained.

From the 156 nodules evaluated with SWE in both planes, the elasticity values obtained at longitudinal orientation were found to be higher than those obtained at transverse orientation for the majority of cases (74.1%). A significant difference was observed for E_{mean} values between longitudinal and transverse measurements with a p <0.0001. E_{max} values in the same way were statistically significantly different when comparing longitudinal and transverse views, with p=0.0002. Figure 2 depicts the longitudinal and transverse cross-section of a benign nodule. Higher elasticity is observed on the longitudinal plane.

A statistically significant difference (p<0.0001) between elasticity measurements from benign and malignant thyroid nodules (Bethesda II and VI) was observed when analyzing each imaging plane individually and after averaging the values from both planes. Table 2 shows the summary of the SWE results for mean and maximum elasticity measurements at longitudinal (L) and transverse (T) probe orientations, average of both orientations only for nodules with measurements from both cross-sections (L∩T), and for all measurements (L∪T). In figure 3, the data distribution can be observed with the measurements obtained from all patients (L∪T) for mean and maximum elasticity values. Furthermore, the difference between a benign and a malignant thyroid nodule under ultrasound SWE can be seen in figure 4.

ROC Analysis

ROC analysis of mean and maximum elasticity values for L, T, L∩T, and L∪T were obtained and are summarized in table 3 for Bethesda categories II and VI (benign and malignant FNA results).

All the parameters analyzed proved to be good predictors for malignancy. However, a large difference between cutoff values from longitudinal and transverse planes was seen particularly for maximum elasticity parameters.

Ultrasound features

Pathological changes in the thyroid gland were analyzed to investigate their effects on elasticity values of thyroid nodules. Table 4 shows the E_{mean}-LUT values of thyroid nodules in presence and absence of goiter, Greaves' disease and heterogeneous thyroid gland. Two malignant cases (NA column) were not included in the Student's t-test analysis since the nodules were not surrounded by thyroid gland (thyroidectomy patients). Additionally, in five benign cases (NA column) the entire gland was replaced by multiple nodules, thus, were not included in the Student's t-test analysis of heterogeneous thyroid gland. Benign nodules in patients with goiter were found to have a statistically significant lower mean elasticity values ($p<0.05$) than nodules within a normal thyroid gland.

In addition, nodule size and internal features of the nodules such as presence of calcifications, cystic component, and vascularity were analyzed. Figure 6 shows a bar plot of nodules containing macrocalcifications and microcalcifications within the SWE imaging plane, and nodules without calcifications. From the benign group 30 nodules had macrocalcifications, SWE imaging of macrocalcifications was avoided in 12 nodules, therefore, the bar plot shows the results from the remaining 18 nodules. 9 nodules had microcalcifications and 73 nodules did not have calcifications. The 12 nodules imaged only on the soft component from the macrocalcifications group were added to the non-calcified group; thus, the benign – not present bar includes 85 nodules. From the malignant group 5 nodules had macrocalcifications, 4 nodules had microcalcifications and 13 nodules did not have calcifications.

Benign nodules with macro or microcalcifications were found to have significantly higher elasticity values compared to benign nodules without calcifications. These results correlate with previous findings (31). Figure 7 shows an example of a false positive benign nodule by SWE containing macrocalcifications.

Table 5 shows the results from the analysis of nodule size, presence of cystic component, and presence of vascularity obtained from E_{mean}-LUT values. The average size of thyroid nodules was 24.89±15.41mm (malignant nodules: 16.95±8.58mm, range 5–34mm and benign nodules: 26.02±14.17mm, range 5–68mm). A statistically significant difference was observed between small and large benign nodules where smaller nodules presented higher elasticity values, however, after overlooking all the nodules with calcifications, the two groups did not show a significant difference ($p=0.5129$). Furthermore, thyroid nodules with a vascular component were found to be softer than solid nodules ($p=0.0489$).

Discussion

In this work, CUSE was used to study the differences between benign and malignant thyroid nodules in terms of elasticity. The results showed that ultrasound SWE could be used as a complementary tool to conventional B-mode imaging for the differentiation of thyroid

nodules. Good sensitivity and specificity were obtained by measurements in the longitudinal view, transverse view, or their combination. In a previous study, Gangadhar et al. (32) concluded that there was moderate to good agreement between values from longitudinal and transverse orientations in thyroid nodules. However, in this study it was observed that elasticity measurements from longitudinal orientation were significantly higher than those taken from transverse orientation. This effect could be due to the anisotropic nature of the muscles that lay on top of the thyroid gland (33, 34). At longitudinal orientation the traveling direction of shear waves is parallel to the orientation of the muscle fibers, thus, potentially increasing the speed of shear waves on the underlying thyroid gland (Fig. 2). Conversely, at transverse orientation the direction of shear waves is perpendicular to the direction of muscle fibers, which may decrease the speed of the waves. A second observation is that at transverse orientation the common carotid artery generates a large pulsatile motion. This pulsation has been previously studied as an intrinsic source of compression to estimate strain in thyroid nodules (35, 36). Therefore, the artery motion may be large enough to interfere with the shear waves traveling through the nodule and create a bias in the final measurement; furthermore, lower intraclass correlations were observed among acquisitions at transverse orientation compared to longitudinal. The difference in measurements from longitudinal and transverse views was also reflected on the cutoff values obtained from E_{mean} (longitudinal-cutoff = 48.40 kPa; transverse-cutoff = 40.63 kPa) and E_{max} (longitudinal-cutoff = 108.48 kPa; transverse-cutoff = 82.69 kPa), where the cutoffs at longitudinal view were significantly higher. Therefore, an indiscriminate use of cutoffs and measurements from different probe orientations could increase the number of false positives or false negatives cases.

Previous studies have reported cutoff values ranging from 34.5 kPa to 90.34 kPa for mean elasticity (22–26, 37). In this study, the optimal E_{mean} cutoff for LUT was 48.40 kPa, which showed a sensitivity of 95.45% and specificity 86.61%. Sensitivity and specificity results are consistent with most of the prior studies. The discrepancy in cutoff values can be attributed to the selection of ROI. In most studies a smaller ROI (1mm or 2mm in diameter) was placed on the stiffest part of the elasticity map. Instead, our measurements were obtained by averaging multiple 3mm-diameter ROIs (up to three), which were placed inside the nodule based on the B-mode image. Using multiple small ROIs instead of one large ROI was previously shown to provide more flexibility in quantification of breast lesions with irregular boundaries (19). The same idea was employed here to acquire SWE values from a larger nodule area without including parenchymal tissue. In terms of lower cutoffs compared to our results, the selection of study population might have a role; in a study by Samir *et al* (38), only thyroid nodules Bethesda categories III and IV were studied under SWE with a final cutoff value of 22.3 kPa. By comparing our cutoff result of 48.40 kPa with the mean values of Bethesda groups III and IV in Table 1 it can be observed that all values are below the threshold, thus, we hypothesize that including other Bethesda groups in the statistical analysis may lower the cutoff values. A good agreement between the study findings and results from previous works (26) was observed in that malignant nodules presented higher elasticity values than benign nodules. Nevertheless, benign nodules with macrocalcifications were significantly stiffer than nodules with microcalcifications, and nodules with microcalcifications were significantly stiffer than nodules with no calcifications.

Furthermore, from the 16 thyroid nodules identified as false positives cases, 9 (56.25%) nodules contained macrocalcifications and 2 (12.5%) nodules had microcalcifications. Thus, benign nodules with calcifications can be perceived as malignant nodules based on ultrasound SWE (31). Additional nodule features such as cystic component and nodule size did not have an effect on shear wave speed measurements among benign and malignant nodules; on the other hand, benign nodules in patients with goiter and benign nodules with a vascular component (identified by using color Doppler imaging) showed reduced elasticity compared to nodules inside normal size thyroid glands and avascular nodules, respectively.

There were some limitations to this study. One of the main limitations was the low number of thyroid carcinomas compared to the larger sample size of benign nodules; however, due to the prospective nature of this study, the population is a reflection of the malignancy rate in thyroid nodules. Bethesda categories I, III, IV and V could not be classified as benign or malignant, thus, 39 nodules were excluded from the statistical analysis. Lastly, the reproducibility of 2D-SWE images has been previously shown to be very high (39); which correlate with our results. Nevertheless, a consensus for the number of SWE acquisitions for thyroid nodules is not determined yet (30); in this study, even though we considered three images per plane, increasing the number of SWE acquisitions might enhance the overall robustness and reproducibility of this diagnostic tool for the differentiation of thyroid nodules.

Conclusions

The quantitative information obtained from the elastic properties of thyroid nodules showed promising results for the discrimination between malignant and benign nodules, where malignant nodules were significantly stiffer than benign nodules. Some factors such as probe orientation and calcifications may change the nodule elasticity value. However, by using a single orientation or average of both orientations, the effect of probe orientation can be accounted for. Calcifications, on the other hand, may lead to perceiving benign nodules as malignant under ultrasound SWE. A larger number of malignant nodules need to be studied to further validate our results.

Acknowledgments

This work was supported by the National Institutes of Health grants: 1R01EB017213 from National Institute of Biomedical Imaging and Bioengineering, as well as grants R01CA148994, R01CA148994-S1, R01CA168575, R01EB017213 and R01CA174723 from the National Cancer Institute. The authors are grateful to Theresa Nelson, Cynthia Andrist and Barbara Foreman for their assistance in patient recruitment.

References

1. Lin J-D, Chao T-C, Huang B-Y, Chen S-T, Chang H-Y, Hsueh C. Thyroid cancer in the thyroid nodules evaluated by ultrasonography and fine-needle aspiration cytology. Thyroid. 2005; 15(7): 708–17. [PubMed: 16053388]
2. Mandel SJ. A 64-year-old woman with a thyroid nodule. Jama. 2004; 292(21):2632–42. [PubMed: 15572721]
3. Khadra H, Bakeer M, Hu T, Kandil E. Vascular flow a predictor of malignant thyroid nodules: a meta-analysis. Journal of the American College of Surgeons. 2014; 219(4):e87–e8.

4. Moon HJ, Kwak JY, Kim MJ, Son EJ, Kim E-K. Can vascularity at power Doppler US help predict thyroid malignancy? Radiology. 2010; 255(1):260–9. [PubMed: 20308462]
5. Haugen BR, Alexander EK, Bible KC, Doherty GM, Mandel SJ, Nikiforov YE, et al. 2015 American Thyroid Association management guidelines for adult patients with thyroid nodules and differentiated thyroid cancer: the American Thyroid Association guidelines task force on thyroid nodules and differentiated thyroid cancer. Thyroid. 2016; 26(1):1–133. [PubMed: 26462967]
6. Anil G, Hegde A, Chong FV. Thyroid nodules: risk stratification for malignancy with ultrasound and guided biopsy. Cancer Imaging. 2011; 11(1):209. [PubMed: 22203727]
7. Hershman JM. Malignancy of a Thyroid nodule can be predicted by ultrasonography if it has microcalcifications and is solid and larger than 2 cm. JAMA. 2013
8. Lyshchik A, Moses R, Barnes SL, Higashi T, Asato R, Miga MI, et al. Quantitative analysis of tumor vascularity in benign and malignant solid thyroid nodules. Journal of ultrasound in medicine. 2007; 26(6):837–46. [PubMed: 17526616]
9. Moon W-J, Jung SL, Lee JH, Na DG, Baek J-H, Lee YH, et al. Benign and malignant thyroid nodules: US differentiation—multicenter retrospective study 1. Radiology. 2008; 247(3):762–70. [PubMed: 18403624]
10. Frates MC, Benson CB, Charboneau JW, Cibas ES, Clark OH, Coleman BG, et al. Management of thyroid nodules detected at US: Society of Radiologists in Ultrasound Consensus Conference Statement 1. Radiology. 2005; 237(3):794–800. [PubMed: 16304103]
11. Brito JP, Gionfriddo MR, Al Nofal A, Boehmer KR, Leppin AL, Reading C, et al. The accuracy of thyroid nodule ultrasound to predict thyroid cancer: systematic review and meta-analysis. The Journal of Clinical Endocrinology & Metabolism. 2013; 99(4):1253–63. [PubMed: 24276450]
12. Nikiforov YE, Ohori NP, Hodak SP, Carty SE, LeBeau SO, Ferris RL, et al. Impact of mutational testing on the diagnosis and management of patients with cytologically indeterminate thyroid nodules: a prospective analysis of 1056 FNA samples. The Journal of Clinical Endocrinology & Metabolism. 2011; 96(11):3390–7. [PubMed: 21880806]
13. Polyzos SA, Anastasilakis AD. Clinical complications following thyroid fine-needle biopsy: a systematic review. Clinical Endocrinology. 2009; 71(2):157–65. [PubMed: 19170717]
14. Cibas ES, Ali SZ. The Bethesda System for Reporting Thyroid Cytopathology. American Journal of Clinical Pathology. 2009; 132(5):658–65. [PubMed: 19846805]
15. Bessey LJ, Lai NBK, Coorough NE, Chen H, Sippel RS. The incidence of thyroid cancer by FNA varies by age and gender. The Journal of surgical research. 2013; 184(2):761–5. [PubMed: 23623584]
16. Yang J, Schnadig V, Logrono R, Wasserman PG. Fine-needle aspiration of thyroid nodules: A study of 4703 patients with histologic and clinical correlations. Cancer Cytopathology. 2007; 111(5):306–15. [PubMed: 17680588]
17. Sarvazyan AP, Rudenko OV, Swanson SD, Fowlkes JB, Emelianov SY. Shear wave elasticity imaging: a new ultrasonic technology of medical diagnostics. Ultrasound in medicine & biology. 1998; 24(9):1419–35. [PubMed: 10385964]
18. Berg WA, Cosgrove DO, Doré CJ, Schäfer FK, Svensson WE, Hooley RJ, et al. Shear-wave elastography improves the specificity of breast US: the BE1 multinational study of 939 masses. Radiology. 2012; 262(2):435–49. [PubMed: 22282182]
19. Bayat M, Denis M, Gregory A, Mehrmohammadi M, Kumar V, Meixner D, et al. Diagnostic features of quantitative comb-push shear elastography for breast lesion differentiation. PLOS ONE. 2017; 12(3):e0172801. [PubMed: 28257467]
20. Ferraioli G, Tinelli C, Dal Bello B, Zicchetti M, Filice G, Filice C. Accuracy of real-time shear wave elastography for assessing liver fibrosis in chronic hepatitis C: A pilot study. Hepatology. 2012; 56(6):2125–33. [PubMed: 22767302]
21. Palmeri ML, Wang MH, Rouze NC, Abdelmalek MF, Guy CD, Moser B, et al. Noninvasive evaluation of hepatic fibrosis using acoustic radiation force-based shear stiffness in patients with nonalcoholic fatty liver disease. Journal of hepatology. 2011; 55(3):666–72. [PubMed: 21256907]
22. Sebag F, Vaillant-Lombard J, Berbis J, Griset V, Henry J, Petit P, et al. Shear wave elastography: a new ultrasound imaging mode for the differential diagnosis of benign and malignant thyroid

nodules. The Journal of Clinical Endocrinology & Metabolism. 2010; 95(12):5281–8. [PubMed: 20881263]

23. Bhatia KS, Tong CS, Cho CC, Yuen EH, Lee YY, Ahuja AT. Shear wave elastography of thyroid nodules in routine clinical practice: preliminary observations and utility for detecting malignancy. European radiology. 2012; 22(11):2397–406. [PubMed: 22645042]
24. Veyrieres J-B, Albarel F, Lombard JV, Berbis J, Sebag F, Oliver C, et al. A threshold value in Shear Wave elastography to rule out malignant thyroid nodules: a reality? European journal of radiology. 2012; 81(12):3965–72. [PubMed: 23031543]
25. Kim H, Kim J-A, Son EJ, Youk JH. Quantitative assessment of shear-wave ultrasound elastography in thyroid nodules: diagnostic performance for predicting malignancy. European radiology. 2013; 23(9):2532–7. [PubMed: 23604801]
26. Zhang B, Ma X, Wu N, Liu L, Liu X, Zhang J, et al. Shear Wave Elastography for Differentiation of Benign and Malignant Thyroid Nodules. Journal of Ultrasound in Medicine. 2013; 32(12): 2163–9. [PubMed: 24277899]
27. Mehrmohammadi M, Denis M, Song P, Chen S, Fatemi M, Alizad A, editorsUltrasonics Symposium (IUS), 2014 IEEE International. IEEE; 2014. Comb-Push Ultrasound Shear Elastography of thyroid: Preliminary in vivo human study.
28. Song P, Urban MW, Manduca A, Zhao H, Greenleaf JF, Chen S. Comb-push ultrasound shear elastography (CUSE) with various ultrasound push beams. IEEE transactions on medical imaging. 2013; 32(8):1435–47. [PubMed: 23591479]
29. Song P, Macdonald MC, Behler RH, Lanning JD, Wang MH, Urban MW, et al. Two-dimensional shear-wave elastography on conventional ultrasound scanners with time-aligned sequential tracking (TAST) and comb-push ultrasound shear elastography (CUSE). IEEE transactions on ultrasonics, ferroelectrics, and frequency control. 2015; 62(2):290–302.
30. Cosgrove D, Barr R, Bojunga J, Cantisani V, Chammas MC, Dighe M, et al. WFUMB guidelines and recommendations on the clinical use of ultrasound elastography: Part 4. thyroid. Ultrasound in medicine & biology. 2017; 43(1):4–26. [PubMed: 27570210]
31. Gregory A, Mehrmohammadi M, Denis M, Bayat M, Stan DL, Fatemi M, et al. Effect of calcifications on breast ultrasound shear wave elastography: an investigational study. PloS one. 2015; 10(9):e0137898. [PubMed: 26368939]
32. Gangadhar K, Hippe DS, Thiel J, Dighe M. Impact of Image Orientation on Measurements of Thyroid Nodule Stiffness Using Shear Wave Elastography. Journal of Ultrasound in Medicine. 2016; 35(8):1661–7. [PubMed: 27335441]
33. Gennisson J-L, Deffieux T, Macé E, Montaldo G, Fink M, Tanter M. Viscoelastic and anisotropic mechanical properties of in vivo muscle tissue assessed by supersonic shear imaging. Ultrasound in medicine & biology. 2010; 36(5):789–801. [PubMed: 20420970]
34. Eby SF, Song P, Chen S, Chen Q, Greenleaf JF, An K-N. Validation of shear wave elastography in skeletal muscle. Journal of biomechanics. 2013; 46(14):2381–7. [PubMed: 23953670]
35. Kim M-H, Luo S, Ko SH, Bae J-S, Lim J, Lim D-J, et al. Thyroid nodule parameters influencing performance of ultrasound elastography using intrinsic compression. Ultrasound in medicine & biology. 2015; 41(9):2333–9. [PubMed: 26095532]
36. Cho YJ, Ha EJ, Han M, Choi JW. US Elastography Using Carotid Artery Pulsation May Increase the Diagnostic Accuracy for Thyroid Nodules with US-Pathology Discordance. Ultrasound in Medicine & Biology. 2017
37. Park AY, Son EJ, Han K, Youk JH, Kim J-A, Park CS. Shear wave elastography of thyroid nodules for the prediction of malignancy in a large scale study. European Journal of Radiology. 2015; 84(3):407–12. [PubMed: 25533720]
38. Samir AE, Dhyani M, Anvari A, Prescott J, Halpern EF, Faquin WC, et al. Shear-wave elastography for the preoperative risk stratification of follicular-patterned lesions of the thyroid: diagnostic accuracy and optimal measurement plane. Radiology. 2015; 277(2):565–73. [PubMed: 25955578]
39. Cosgrove DO, Berg WA, Doré CJ, Skyba DM, Henry J-P, Gay J, et al. Shear wave elastography for breast masses is highly reproducible. European Radiology. 2012; 22(5):1023–32. [PubMed: 22210408]

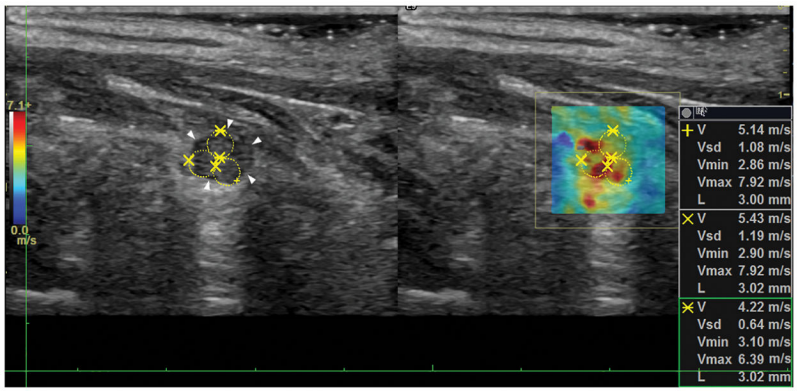

Figure 1.

Recurrent Hurthle cell carcinoma. Longitudinal view of the malignant nodule on the thyroid bed. The white arrows point at the border of the nodule and the yellow circles denote the ROIs for shear wave speed calculation.

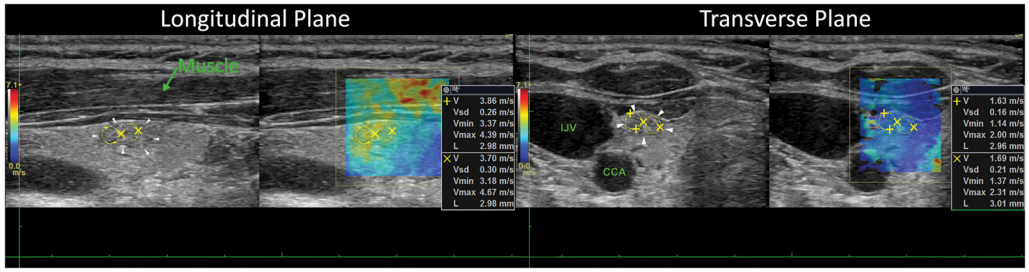

Figure 2.

Longitudinal and transverse view of a benign thyroid nodule. The white arrows point at the border of the nodule and the yellow circles denote the ROIs for shear wave speed calculation.

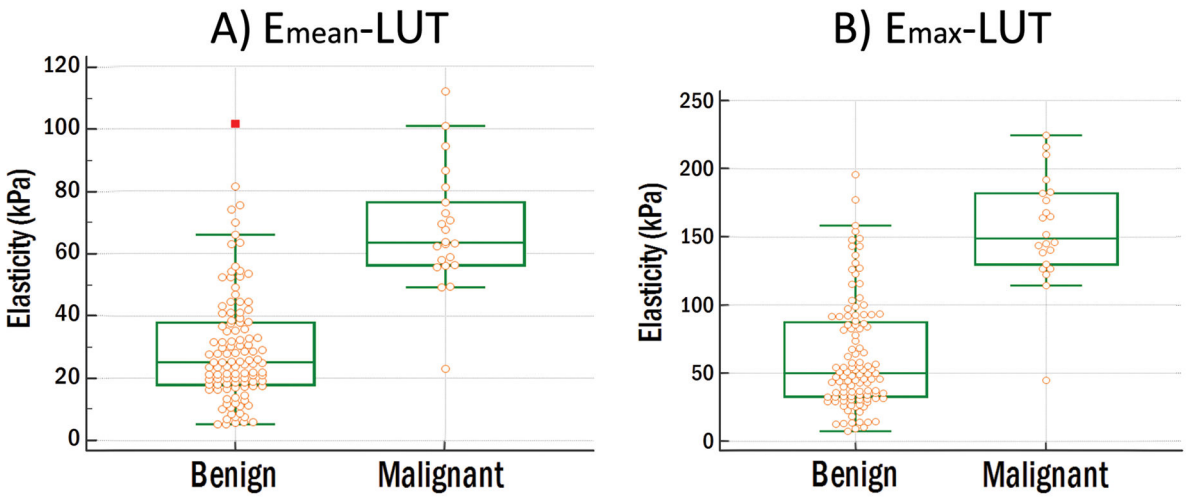

Figure 3.

Data comparison graph of 112 benign nodules and 22 malignant nodules. (**A**) Mean elasticity. Benign: lowest value=5.33 kPa, highest value=101.49 kPa and median=25.17 kPa. Malignant: lowest value=23.07 kPa, highest value=111.81 kPa and median=63.56 kPa. (**B**) Maximum elasticity. Benign: lowest value=7.59 kPa, highest value=195.70 kPa and median=50.00 kPa. Malignant: lowest value=44.90 kPa, highest value=224.47 kPa and median=148.87 kPa.

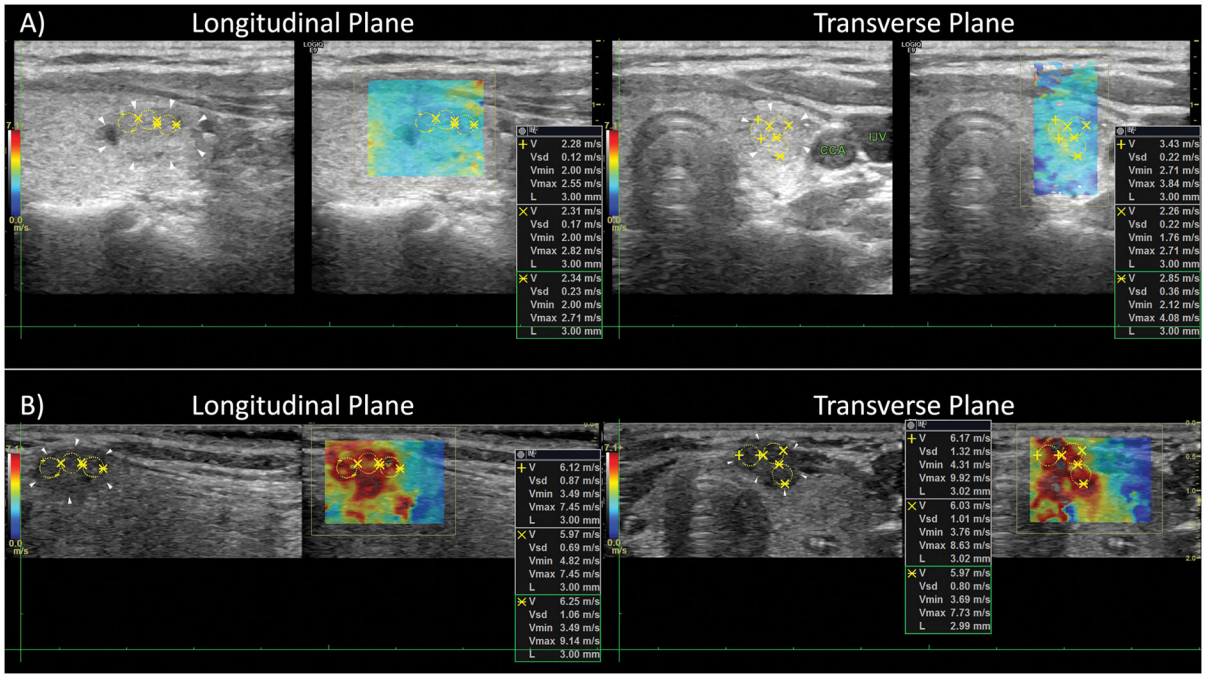

Figure 4.

Longitudinal and transverse view of a benign (**A**) and a maligant (**B**) thyroid nodule. The average elasticity of the two planes resulted in E_{mean}=20.16 kPa and E_{mean}=111.08 kPa for the benign nodule and malignant nodule, respectively.

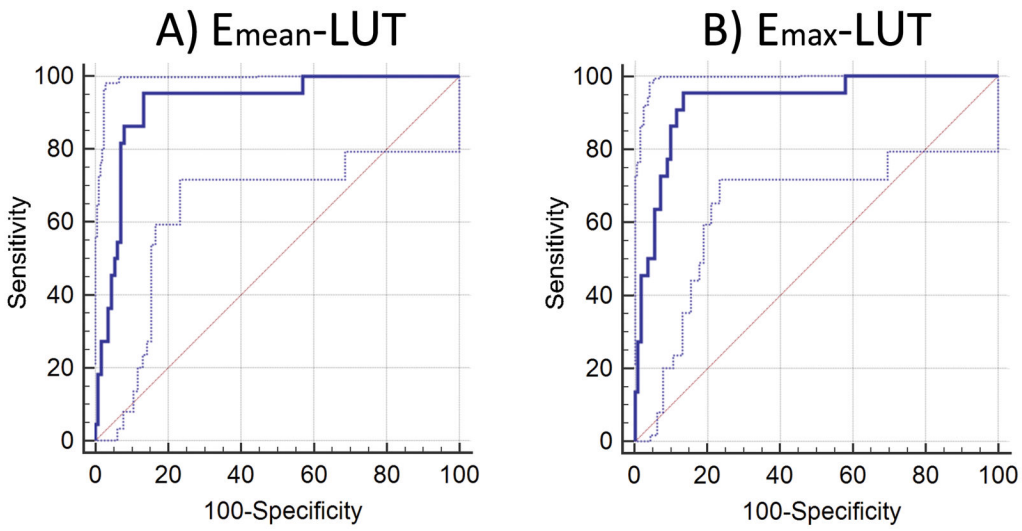

Figure 5.

ROC curve analysis of 134 nodules at longitudinal and transverse planes (LUT) for (**A**) mean elasticity values and (**B**) maximum elasticity values. The dotted blue lines represent the 95% confidence bounds.

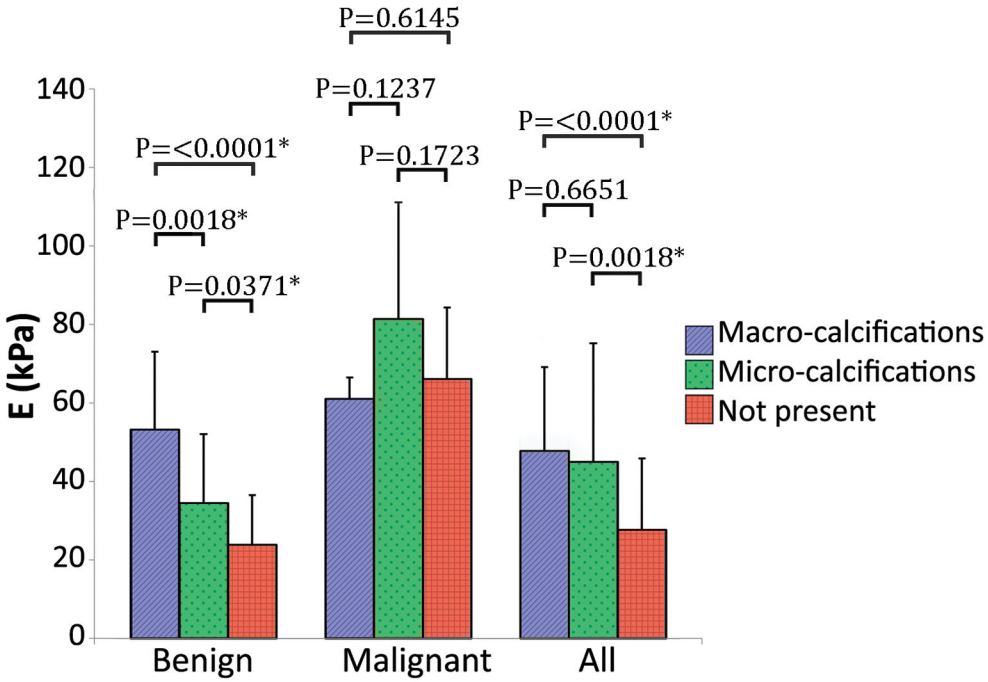

Figure 6.

Student's t-test comparison of elasticity values from nodules containing macrocalcifications (Benign n=18; Malignant n=5; All n=31), microcalcifications (Benign n=9; Malignant n=4; All n=15) and nodules without calcifications (Benign n=85; Malignant n=13; All n=127). All includes Bethesda I, II, III, IV, V, and VI. *p<0.05

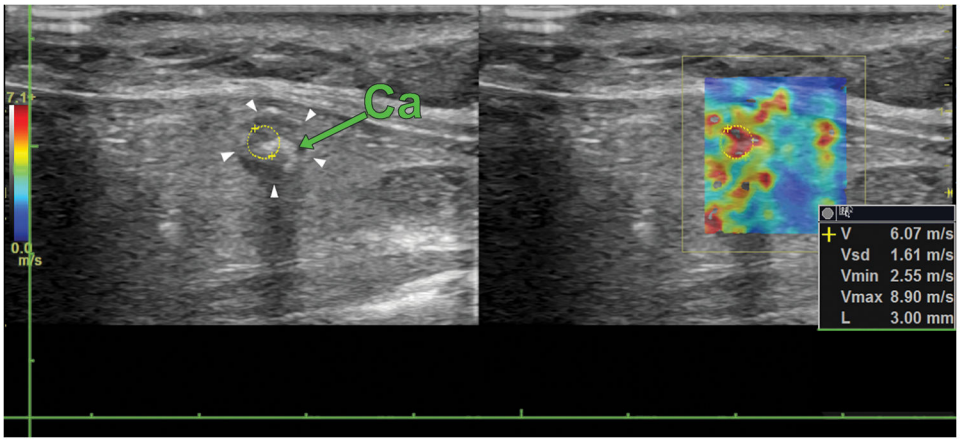

Figure 7.

Longitudinal view of a benign thyroid nodule containing a macrocalcification (green arrow). The white arrows point at the border of the nodule and the yellow circle denotes the ROI for shear wave speed calculation. The elasticity on the nodule is 110.53 kPa.

Table 1

Comb-push shear elastography results compared to sonographic pattern classification and Bethesda Diagnostic category for thyroid nodules.

Classification of thyroid nodules based on sonographic and FNA findings			***Sonographic pattern* (N)**				
			Benign (0)	**Very low suspicion (42)**	**Low suspicion (66)**	**Intermediate suspicion (37)**	**High suspicion (28)**
		Estimated risk of malignancy (%)	< 1	< 3	5–10	10–20	> 70–90
			E_{mean}±SD (kPa)				
***Bethesda Diagnostic Category* (N)**	I (15)	1–4	-	17±7 (6)	17±10 (2)	25±6 (2)	24±12 (5)
	II (112)	0–3	-	29±17 (32)	30±18 (53)	26±18 (20)	40±19 (7)
	III (1)	5–15	-	-	-	12 (1)	-
	IV (20)	15–30	-	20±14 (4)	26±13 (8)	19±3 (4)	15±4 (4)
	V (3)	60–75	-	-	35±8 (2)	63 (1)	-
	VI (22)	97–99	-	-	59 (1)	62±22 (9)	73±17 (12)
			E_{max}±SD (kPa)				
***Bethesda Diagnostic Category* (N)**	I (15)	1–4	-	44±31 (6)	40±30 (2)	47±10 (2)	60±31 (5)
	II (112)	0–3	-	58±35 (32)	60±36 (53)	57±54 (20)	94±48 (7)
	III (1)	5–15	-	-	-	23 (1)	-
	IV (20)	15–30	-	35±24 (4)	43±18 (8)	46±28 (4)	27±4 (4)
	V (3)	60–75	-	-	73±29 (2)	145 (1)	-
	VI (22)	97–99	-	-	114 (1)	147±49 (9)	164±31 (12)

(N) indicates statistical frequency; E_{mean}, mean elasticity; E_{max}, maximum elasticity.

I - Nondiagnostic or Unsatisfactory

II – Benign

III - Atypia of Undetermined Significance or Follicular Lesion of Undetermined Significance

IV - Follicular Neoplasm or Suspicious for a Follicular Neoplasm

V - Suspicious for Malignancy

VI - Malignant

Table 2

Comparison of benign and malignant elasticity measurements (mean ± standard deviation) at longitudinal, transverse and combination of views.

		L	(N=130)	T	(N=126)	L∩T	(N=122)	L∪T	(N=134)
E_{mean}±SD *(kPa)*	Benign	33.09±22.28	(108)	25.41±16.37	(109)	28.92±17.48	(105)	29.53±17.89	(112)
	Malignant	72.64±21.81	(22)	57.94±17.22	(17)	64.26±16.04	(17)	67.76±19.21	(22)
	p-value	<0.0001 *		<0.0001 *		<0.0001 *		<0.0001 *	
E_{max}±SD *(kPa)*	Benign	66.87±44.37	(108)	56.01±41.38	(109)	60.23±37.42	(105)	62.53±40.57	(112)
	Malignant	161.29±42.08	(22)	139.05±52.68	(17)	147.12±39.52	(17)	155.05±39.75	(22)
	p-value	<0.0001 *		<0.0001 *		<0.0001 *		<0.0001 *	

N indicates statistical frequency; E_{mean}, mean elasticity; E_{max}, maximum elasticity; L, Longitudinal; T, Transverse; L∩T, group of nodules with transverse and longitudinal measurements; L∪T, group of nodules with transverse and/or longitudinal measurements.

* $p<0.05$

Table 3

Comparison of CUSE diagnostic performance respect to elasticity parameters and transducer orientation for Bethesda category II and VI.

	Cutoff (kPa)	AUC (95% CI)	Sensitivity (95% CI)	Specificity (95% CI)
E_{mean}-L	48.40	0.91 (0.851 – 0.955)	95.45% (77.2 – 99.9)	83.33% (74.9 – 89.8)
E_{mean}-T	40.63	0.91 (0.840 – 0.950)	94.12% (71.3 – 99.9)	84.04% (76.2– 90.6)
E_{max}-L	108.48	0.92 (0.864 – 0.963)	95.45% (77.2 – 99.9)	84.04% (79.2 – 92.7)
E_{max}-T	82.69	0.90 (0.829 – 0.943)	94.12% (71.3 – 99.9)	78.90% (70.0 – 86.1)
E_{mean}-L∩T	49.09	0.92(0.857 – 0.962)	94.12% (71.3 – 99.9)	86.67% (78.6 – 92.5)
E_{max}-L∩T	103.72	0.93(0.864 – 0.966)	94.12% (71.3 – 99.9)	87.62% (79.8 – 93.2)
E_{mean}-L∪T	49.09	0.92 (0.864 – 0.962)	95.45% (77.2 – 99.9)	86.61% (78.9 – 92.3)
E_{max}-L∪T	105.61	0.93 (0.872 – 0.966)	95.45% (72.2 – 99.9)	86.61% (78.9 – 92.3)

AUC, area under the curve; CI, confidence interval; E_{mean}, mean elasticity; E_{max}, maximum elasticity; L, Longitudinal; T, Transverse; L∩T,: group of nodules with transverse and longitudinal measurements; L∪T, group of nodules with transverse and/or longitudinal measurements.

Table 4

Comparison of mean elasticity measurements (in kPa) with respect to goiter, Graves' disease and heterogeneous thyroid gland.

Thyroid gland Pathologies		Yes (kPa)	N	No (kPa)	N	*p*-value	NA (kPa)	N
Goiter	Benign	23.22±13.82	(30)	31.84±18.71	(82)	0.0125 *	-	(0)
	Malignant	94.34	(1)	65.64±19.51	(19)	0.1572	74.66±2.46	(2)
	All	23.41±16.89	(41)	35.39±21.79	(129)	0.0018 *	51.99±39.29	(3)
Graves' Disease	Benign	31.12±11.76	(3)	29.49±18.06	(109)	0.6459	-	(0)
	Malignant	-	(0)	67.07±20.05	(20)	-	74.66±2.46	(2)
	All	31.12±11.76	(3)	33.02±21.45	(167)	0.8798	51.99±39.29	(3)
Heterogeneous thyroid gland	Benign	34.22±24.37	(15)	29.00±16.58	(92)	0.2982	25.30±20.80	(5)
	Malignant	-	(0)	67.07±20.05	(20)	-	74.66±2.46	(2)
	All	31.23±23.29	(18)	32.90±21.16	(147)	0.7355	25.30±20.80 51.99±39.29	(5) (3)

N indicates statistical frequency; NA, not apply (results excluded from t-test); All includes Bethesda categories I, II, III, IV, V, and VI.

* $p<0.05$

Table 5

Comparison of mean elasticity measurements (in kPa) with respect to nodule size, and presence of cystic and vascular components.

Nodule Features		*<25mm*	*N*	*>=25mm*	*N*	*p-value*
Nodule size	Benign	33.91±19.13	(62)	24.11±14.66	(50)	0.0035*
	Malignant	67.26±20.02	(17)	69.47±18.10	(5)	0.8278
	All	37.49±22.57	(103)	25.98±18.40	(70)	0.0005*
		Yes (kPa)	***N***	***No (kPa)***	***N***	***p-value***
Cystic component	Benign	28.82±18.07	(61)	30.39±17.81	(51)	0.5338
	Malignant	62.20	(1)	68.03±19.64	(21)	0.6935
	All	27.23±17.99	(72)	36.83±23.24	(101)	0.0039*
		Yes (kPa)	***N***	***No (kPa)***	***N***	***p-value***
Vascularity	Benign	23.86±14.55	(27)	31.33±18.54	(85)	0.0403*
	Malignant	54.90±18.89	(5)	71.55±18.11	(17)	0.2246
	All	27.12±17.12	(44)	34.79±22.77	(129)	0.0489*

N indicates statistical frequency; All includes Bethesda categories I, II, III, IV, V, and VI.

* $p<0.05$